JOURNAL OF COMPUTATIONAL PHYSICS **143,** 181–199 (1998)
ARTICLE NO. CP985959

Multidimensional Upwinding. Part II. Decomposition of the Euler Equations into Advection Equations

Michael Fey

Seminar for Applied Mathematics, ETH-Zürich, CH-8092, Zürich, Switzerland
E-mail: fey@sam.math.ethz.ch

Received September 25, 1997; revised February 9, 1998

Based on a genuine multidimensional numerical scheme, called the Method of Transport, we derive a form of the compressible Euler equations, capable of a linearization for any space dimension. This form enables a rigorous error analysis of the linearization error without the knowledge of the numerical method used to solve the linear equations. The generated error can be eliminated by special correction terms in the linear equations. Hence, existing scalar high order methods can be used to solve the linear equations and obtain high order accuracy in space and time for the non-linear conservation law. In this approach, the scalar version of the method of transport is used to solve the linear equations. This method is multidimensional and reduces the solution of the partial differential equation to an integration process. Convergence histories presented at the end of the paper show that the numerical results agree with the theoretical predictions.

1. INTRODUCTION

For the class of scalar conservation laws, the theory of convergence and stability is well established for a large number of numerical methods. This is also true in view of error estimates and convergence properties, i.e., the order of convergence. Even for multidimensional calculations, there are more and more attempts to design high order schemes [1, 7, 12].

For the class of systems of conservation laws, the situation is quite different. For most of the existing schemes, there are only heuristic arguments, that these methods are of the same order as their scalar counterparts. Some approaches, like the Strang [10] splitting for multidimensional computations, are limited to second order accuracy by construction.

To obtain a high order method for systems, it is necessary to take into account all sources of errors. In several space dimensions, there is mainly the dimension splitting error that

0021-9991/98 $25.00

restricts the order to at most two. But even in one space dimension, the error arising from the linearization of a non-linear system plays an important role. This kind of error is introduced if the method relies on an approximate Riemann solver, e.g., flux-difference or flux-vector splitting.

Based on the derivation of a multidimensional method, called the Method of Transport (MoT), a new form of the compressible Euler equations called the advection form is introduced that allows a multidimensional linearization, i.e., decoupling into a number of advection equations.

This formalism allows us to compare the Taylor expansion of the exact solution at time $t + \Delta t$ after one time step with the expansion of the exact solution of the linearized equations, in order to obtain the splitting and truncation errors. It simplifies a rigorous error analysis and makes it visible. This decomposition also provides a general frame work for the solution of hyperbolic conservation laws, since the solution of a non-linear system is reduced to the solution of linear scalar equations if such a decomposition exists. It is also independent of the numerical method or the space discretization used to solve the linear equations, i.e., finite volume or finite element methods on structured or unstructured grids.

A direct comparison of the linearized equations and the non-linear Euler equations shows that the local approximation error is $O(\Delta t^2)$, i.e., we obtain a first order approximation of the non-linear system independent of the spatial discretization. Because of the special structure of the error terms they can be integrated into the linear equations to eliminate the resulting approximation error. These correction terms, added to the scalar advection equation, do not change the character of the equations, nor is their influence limited to a second order correction. It has been verified that these correction terms exist for the Euler equations at least up to third order accuracy.

In this paper we first recall the process of linearization in one space dimension for the flux-vector splitting methods [9]. Then, using the ideas of the MoT we derive a simple decomposition of the multidimensional Euler equations into a set of linear advection equations. To obtain the linearization error in the smooth part of the solution we compare the Taylor expansions of both solutions. We will explain this procedure for the conservation of mass in 1-D only and give the results for the 1-D and the 2-D case.

We then briefly introduce a numerical algorithm to solve these equations efficiently and to high order of accuracy. In some numerical experiments at the end, we verify the theoretical results. Convergence histories for smooth solutions in one and two space dimensions illustrate the influence of the second order correction terms. A solution of a Mach 10 flow indicates the robustness of the method even for strong shocks.

2. LINEARISATION OF THE EQUATIONS IN 1-D

For a better understanding of the multidimensional linearization process we first explain the same steps in one space dimension. For this we have to stress the idea of flux-vector splitting again. This time we focus on the linearization of a non-linear system.

The one-dimensional compressible Euler equations in conservation form can be written as

$$\frac{\partial}{\partial t}\mathbf{U} + \frac{\partial}{\partial x}\mathbf{F}(\mathbf{U}) = 0, \tag{1}$$

where **U** is the state vector of the conserved quantities and **F(U)** is the flux given by

$$\mathbf{U} = \begin{pmatrix} \rho \\ m \\ E \end{pmatrix}, \qquad \mathbf{F}(\mathbf{U}) = \begin{pmatrix} m \\ \rho u^2 + p \\ u(E+p) \end{pmatrix}.$$

Here, ρ is the mass density, $m = \rho u$ is the momentum, E is the total energy, u is the velocity, and p is the pressure related to **U** by the equation of state

$$p = (\gamma - 1)\left(E - \rho\frac{u^2}{2}\right).$$

The ration of the specific heat capacities γ takes the value 1.4 for air.

The quasi-linear form of (1) is given by

$$\mathbf{U}_t + \frac{\partial \mathbf{F}}{\partial \mathbf{U}}\mathbf{U}_x =: \mathbf{U}_t + \boldsymbol{A}\mathbf{U}_x = 0.$$

Since Eq. (1) is hyperbolic, the matrix $\boldsymbol{A}$ has only real eigenvalues and a full set of eigenvectors. Thus, the Jacobian matrix $\boldsymbol{A}$ can be diagonalized by the matrix $\boldsymbol{R}$ of right eigenvectors. We have the relation

$$\boldsymbol{A} = \boldsymbol{R}\boldsymbol{\Lambda}\boldsymbol{R}^{-1} \qquad \text{or} \qquad \boldsymbol{\Lambda} = \boldsymbol{R}^{-1}\boldsymbol{A}\,\boldsymbol{R},$$

where $\boldsymbol{\Lambda} = \mathrm{diag}(\lambda_1, \lambda_2, \lambda_3) = \mathrm{diag}(u + c, u, u - c)$.

The homogeneity of the Euler equations can be used to write to flux **F** as

$$\mathbf{F}(\mathbf{U})\frac{\partial \mathbf{F}}{\partial \mathbf{U}}\mathbf{U} =: \boldsymbol{A}\mathbf{U} = \boldsymbol{R}\boldsymbol{\Lambda}\boldsymbol{R}^{-1}\mathbf{U} = \sum_{i=1}^{3}(\alpha_i \mathbf{r}_i)\lambda_i, \tag{2}$$

for any state vector **U**. Here, $\boldsymbol{R} = (\mathbf{r}_1, \mathbf{r}_2, \mathbf{r}_3)$ is the matrix of right eigenvectors of $\boldsymbol{A}$. The vector $\boldsymbol{\alpha} = (\alpha_1, \alpha_2, \alpha_3)^T := \boldsymbol{R}^{-1}\mathbf{U}$ and c is the speed of sound, given by $c^2 = \gamma p/\rho$. Using (2) and the fact that

$$\mathbf{U} = \boldsymbol{I}\mathbf{U} = \underline{\boldsymbol{R}\boldsymbol{R}}^{-1}\mathbf{U} = \sum_{i=1}^{3}(\alpha_i \mathbf{r}_i), \tag{3}$$

i.e., **U** can be decomposed into the same vectors $(\alpha_i \mathbf{r}_i)$ as the flux, (1) becomes

$$\sum_{i=1}^{3}\left(\frac{\partial}{\partial t}(\alpha_i \mathbf{r}_i) + \frac{\partial}{\partial x}((\alpha_i \mathbf{r}_i)\lambda_i)\right) = 0. \tag{4}$$

Equation (4) is called the advection form of the Euler equations. Note that even though (4) formally looks like a sum of advection equations, Eqs. (1) and (4) are the same. No approximation has been made. Writing the full dependencies

$$\sum_{i=1}^{3}\left(\frac{\partial}{\partial t}(\alpha_i(\mathbf{U}(x,t))\mathbf{r}_i(\mathbf{U}(x,t))) + \frac{\partial}{\partial x}((\alpha_i(\mathbf{U}(x,t))\mathbf{r}_i(\mathbf{U}(x,t)))\lambda_i(\mathbf{U}(x,t)))\right) = 0$$

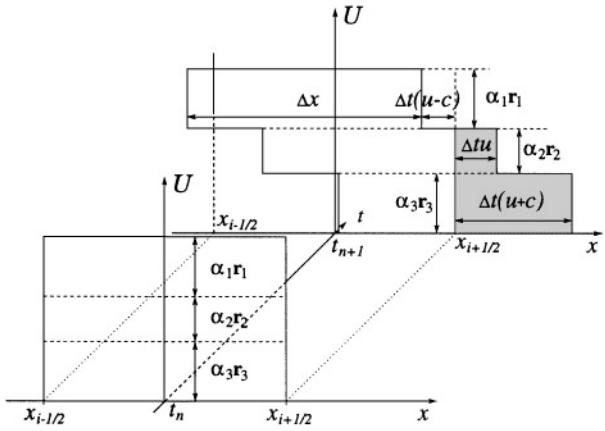

FIG. 1. Decomposition of **U** at time t_n and transport with characteristic speed. The gray region has passed the cell boundary from left to right during time $t_{n+1} - t_n$. Only the right-going flux is indicated.

shows the non-linearity of the system. In the Steger–Warming splitting the different terms in the sum are treated separately. Each part is propagated with its characteristic speed as shown in Fig. 1. From the mathematical point of view the dependencies are changed to

$$\mathbf{s}_i(x,t,0) := (\alpha_i \mathbf{r}_i)(\mathbf{U}(x,t)), \qquad a_i(x,t) := \lambda_i(\mathbf{U}(x,t))$$

together with the evolution equations

$$\frac{\partial}{\partial \tau}\mathbf{s}_i(x,t,\tau) + \frac{\partial}{\partial x}(\mathbf{s}_i(x,t,\tau)\, a_i(x,t)) = 0, \qquad i = 1,2,3.$$

These are now three linear systems or a total of nine scalar advection equations of the form

$$\frac{\partial}{\partial \tau}\omega(x,\tau) + \frac{\partial}{\partial x}(a(x)\omega(x,\tau)) = 0, \tag{5}$$

where ω is one of the components of $\mathbf{s}_i$, $i = 1, 2, 3$, and a is the corresponding characteristic speed λ_i, $i = 1, 2, 3$, which, in this process, becomes a function of space only. The resulting numerical scheme is consistent since the sum of all equations in (5) gives (4). After solving the decoupled scalar equations for a small time step Δt an approximation of the solution of the non-linear system is obtained by adding up the linear solutions. Iteration of this propagation step with updated values of $\mathbf{r}_i$ and λ_i yields the numerical scheme. This can be interpreted as a Huygens principle for short times, i.e., interactions between different "waves" are neglected. The non-linear coupling takes place during the averaging process in the finite volume discretization.

3. LINEARIZATION OF THE 2-D EULER-EQUATIONS

As we have seen in [2], the above approach is not possible in several space dimensions. For example in the 2-D case, the equations have the form

$$\frac{\partial}{\partial t}\mathbf{U} + \frac{\partial}{\partial x}\mathbf{F}_1(\mathbf{U}) + \frac{\partial}{\partial y}\mathbf{F}_2(\mathbf{U}) = 0, \tag{6}$$

with

$$\mathbf{U} = \begin{pmatrix} \rho \\ m \\ n \\ E \end{pmatrix}, \qquad \mathbf{F}_1 = \begin{pmatrix} \rho u \\ \rho u^2 + p \\ \rho uv \\ u(E+p) \end{pmatrix}, \qquad \mathbf{F}_2 = \begin{pmatrix} \rho v \\ \rho uv \\ \rho v^2 + p \\ v(E+p) \end{pmatrix}.$$

Here, $\vec{\boldsymbol{m}} = (m, n)^T$ is the momentum and $\vec{\boldsymbol{u}} = (u, v)^T = (m/\rho, n/\rho)^T$ is the velocity. The pressure p is given by

$$p = (\gamma - 1)\left(E - \rho\frac{u^2 + v^2}{2}\right).$$

The equations are still hyperbolic and a linearization of the form

$$\mathbf{U}_t + \frac{\partial \mathbf{F}_1}{\partial \mathbf{U}}\mathbf{U}_x + \frac{\partial \mathbf{F}_2}{\partial \mathbf{U}}\mathbf{U}_y = 0$$

is possible, but the Jacobian matrices of $\mathbf{F}_1$ and $\mathbf{F}_2$ cannot be diagonalized simultaneously. A number of methods use the one-dimensional decomposition in (4) in each space direction. Let $\boldsymbol{\Lambda} = \boldsymbol{R}^{-1}\boldsymbol{A}\boldsymbol{R}$ be the decomposition of the flux in x-direction with eigenvalues $\boldsymbol{\Lambda} = \mathrm{diag}(\lambda_1, \ldots, \lambda_4)$ and $\boldsymbol{\Xi} = \boldsymbol{S}^{-1}\boldsymbol{B}\boldsymbol{S}$ the decomposition of the flux in y-direction with eigenvalues $\boldsymbol{\Xi} = \mathrm{diag}(\xi_1, \ldots, \xi_4)$. With $\boldsymbol{R} = (\mathbf{r}_1, \ldots, \mathbf{r}_4)$, $\boldsymbol{R}^{-1}\mathbf{U} = (\alpha_1, \ldots, \alpha_4)^T$, $\mathbf{S} = (\mathbf{s}_1, \ldots, \mathbf{s}_4)$, and $\mathbf{S}^{-1}\mathbf{U} = (\beta_1, \ldots, \beta_4)^T$ we can decompose the two one-dimensional problems into

$$\begin{aligned} \sum_{i=1}^{4}((\alpha_i \mathbf{r}_i)_t + (\lambda_i(\alpha_i \mathbf{r}_i))_x) &= \mathbf{U}_t + \mathbf{F}_1(\mathbf{U})_x, \\ \sum_{i=1}^{4}((\beta_i \mathbf{s}_i)_t + (\xi_i(\beta_i \mathbf{s}_i))_y) &= \mathbf{U}_t + \mathbf{F}_2(\mathbf{U})_y, \end{aligned} \tag{7}$$

which corresponds to eight waves. Applying the consistency criteria for multidimensional wave decompositions in [2] to (7) directly shows that

$$\sum_{i=1}^{4}(\alpha_i \mathbf{r}_i + \beta_i \mathbf{s}_i) = 2\mathbf{U} \neq \mathbf{U}.$$

Thus, the decomposition is not consistent in this form. With the simple modification

$$\begin{aligned} \frac{1}{2}\left(\sum_{i=1}^{4}(\alpha_i \mathbf{r}_i)_t + (2\lambda_i(\alpha_i \mathbf{r}_i))_x\right) &= \frac{1}{2}\mathbf{U}_t + \mathbf{F}_1(\mathbf{U})_x, \\ \frac{1}{2}\left(\sum_{i=1}^{4}(\beta_i \mathbf{s}_i)_t + (2\xi_i(\beta_i \mathbf{s}_i))_y\right) &= \frac{1}{2}\mathbf{U}_t + \mathbf{F}_2(\mathbf{U})_y, \end{aligned} \tag{8}$$

we obtain a proper decomposition. The actual operators are almost identical to the one-dimensional ones, except for the factor 2 in front of the characteristic speeds. This explains the lack of stability observed for the "donor" cell approach. The propagation speeds seem

to be twice as high thus resulting in a reduction of the possible time step to 1/2. In three space dimensions the reduction would be 1/3. The same results were obtained by a linear stability analysis in [6].

The MoT derived in [2] provides the necessary information to find a linearization in the multidimensional case. We are not interested in a direction wise decomposition which directly leads to the dimensional splitting approach. Instead, we are seeking an approximation of the non-linear system by a set of linear but multidimensional advection equations equivalent to the 1-D case. First, we will rewrite the Euler equations in a more convenient form. Let

$$\boldsymbol{F}(\mathbf{U}) = \mathbf{U}\mathbf{u}^T + \begin{pmatrix} \vec{\mathbf{0}}^T \\ \boldsymbol{I} \\ \vec{\boldsymbol{u}}^T \end{pmatrix} p \tag{9}$$

be the $(N+2) \times N$ matrix representing the multidimensional flux. N denotes the dimension of the space, $\boldsymbol{I}$ is the $N \times N$ identity matrix, and $\vec{\mathbf{0}}$ is the N-dimensional vector of zeros. Then the general form (6) can be written as

$$\mathbf{U}_t + \nabla \cdot (\boldsymbol{F}(\mathbf{U})) = \mathbf{0}, \tag{10}$$

where the divergence acts on the rows of $\boldsymbol{F}$.

The basic idea generating the acoustic waves in MoT was a Huygens principle, i.e., the superposition of spherical shaped waves. To find a decomposition, a description by planar waves in needed, since this can simply be modeled by advection operators. The MoT uses the definitions

$$\mathbf{R}_1(\mathbf{U}) := \frac{1}{\gamma} \begin{pmatrix} \rho \\ \rho\vec{\boldsymbol{u}} \\ \rho H \end{pmatrix}, \qquad \mathbf{R}_2(\mathbf{U}) := \frac{\gamma - 1}{\gamma} \begin{pmatrix} \rho \\ \rho\vec{\boldsymbol{u}} \\ \rho|\vec{\boldsymbol{u}}|^2/2 \end{pmatrix}, \qquad \boldsymbol{L}(\mathbf{U}) := \frac{\rho c}{\gamma} \begin{pmatrix} \vec{\mathbf{0}}^T \\ \boldsymbol{I} \\ \vec{\boldsymbol{u}}^T \end{pmatrix},$$

where $H = (E + p)/\rho$ denotes total enthalpy and c is the speed of sound. Notice that the newly introduced matrix structure of $\boldsymbol{L}$ is similar to the part in front of the pressure in the multidimensional flux (9). This structure naturally arises in the derivation of MoT.

The solution operator for a multidimensional scalar advection equation of the form

$$\omega_t + \nabla \cdot (\omega \vec{\boldsymbol{a}}^T) = 0 \tag{11}$$

is given by

$$\omega(\vec{\boldsymbol{x}}, t + \Delta t) = \int_{\mathbb{R}^N} \omega(\vec{\boldsymbol{y}}, t)\delta(\vec{\boldsymbol{x}} - \vec{\boldsymbol{z}}(\vec{\boldsymbol{y}}, \Delta t))\, d\vec{\boldsymbol{y}}, \tag{12}$$

where $\vec{\boldsymbol{z}}$ is the solution of

$$\frac{\partial}{\partial \tau}\vec{\boldsymbol{z}}(\vec{\boldsymbol{x}}, \tau) = \vec{\boldsymbol{a}}(\vec{\boldsymbol{z}}(\vec{\boldsymbol{x}}, \tau)) \tag{13}$$

for sufficiently smooth velocity $\vec{\boldsymbol{a}}$. Note that the operator generating the acoustic and advective waves in MoT includes a similar structure. It is obvious for the wave $\mathcal{U}$ given

as

$$\mathcal{U}(\vec{x}, t+\Delta t) = \int_{\mathbb{R}^N} \mathbf{R}_2(\mathbf{U}(\vec{y}, t))\delta(\vec{x} - \vec{z}^u(\mathbf{U}, \vec{y}, \Delta t))\, d\vec{y}. \tag{14}$$

The advection velocity can be identified as flow velocity $\vec{u}$, since $\vec{z}^u$ is the solution to $\dot{\vec{z}}^u = \vec{u}$. In the wave $\mathcal{C}^+$ (and $\mathcal{C}^-$), defined as

$$\mathcal{C}^+(\vec{x}, t+\Delta t) = \frac{1}{|S(1)|} \int_{S(1)} \int_{\mathbb{R}^N} \mathbf{R}_1(\mathbf{U}(\vec{y}, t))\delta(\vec{x} - \vec{z}^c(\mathbf{U}, \vec{y}, \Delta t, \vec{n}))\, ds\, d\vec{y},$$

with $S(1)$ the unit sphere in $\mathbb{R}^N$, the same operator exists. The inner integral formally looks like the advection operator with velocity $\dot{\vec{z}}^c(\mathbf{U}, \vec{y}, \tau, \vec{n}) = \vec{u} + c\vec{n}$. The outer integral averages over all directions $\vec{n}$. Since $\mathcal{C}^+$ and $\mathcal{C}^-$ use the same path $\vec{z}^c$ we can combine them to one wave

$$\begin{aligned}\mathcal{C}(\vec{x}, t+\Delta t) &= \mathcal{C}^+(\vec{x}, t+\Delta t) + \mathcal{C}^-(\vec{x}, t+\Delta t) \\ &= \frac{1}{|S(1)|} \int_{S(1)} \int_{\mathbb{R}^N} (\mathbf{R}_1(\mathbf{U}(\vec{y}, t)) + \boldsymbol{L}(\mathbf{U}(\vec{y}, t)) \cdot \vec{n})\delta(\vec{x} - \vec{z}^c(\mathbf{U}, \vec{y}, \Delta t, \vec{n}))\, ds\, d\vec{y}.\end{aligned} \tag{15}$$

The advection operators in (14) and (15) formally connect the waves to the processes

$$(\mathbf{R}_2)_t + \nabla \cdot (\mathbf{R}_2 \vec{u}^T) = 0$$

for the wave $\mathcal{U}$ and

$$(\mathbf{R}_1 + \boldsymbol{L}\vec{n})_t + \nabla \cdot ((\mathbf{R}_1 + \boldsymbol{L}\vec{n})(\vec{u} + c\vec{n})^T) = 0 \qquad \forall \vec{n} \in S(1)$$

for $\mathcal{C}$. This allows us to rewrite the Euler equations (10) as

$$\frac{\partial}{\partial t}\left(\mathbf{R}_2 + \frac{1}{|S(1)|} \int_{S(1)} (\mathbf{R}_1 + N\boldsymbol{L}\vec{n})\, ds\right) + \nabla \cdot \left(\mathbf{R}_2 \vec{u}^T + \int_{S(1)} (\mathbf{R}_1 + N\boldsymbol{L}\vec{n})(\vec{u} + c\vec{n})^T\, ds\right) = 0. \tag{16}$$

This can easily be verified, since $\mathbf{R}_1$, $\mathbf{R}_2$, and $\boldsymbol{L}$ do not depend on $\vec{n}$, the relations

$$\mathbf{R}_1 + \mathbf{R}_2 = \mathbf{U} \qquad \text{and} \qquad \int_{S(1)} \boldsymbol{L}\vec{n}\, ds = \mathbf{0}$$

lead to $\mathbf{U}$ in the first part. From this we also get that

$$\mathbf{R}_2 \vec{u}^T + \frac{1}{|S(1)|} \int_{S(1)} \mathbf{R}_1 (\vec{u} + c\vec{n})^T ds = \mathbf{U}\vec{u}^T$$

while the parts including $\boldsymbol{L}$ give

$$\frac{N}{|S(1)|} \int_{S(1)} \boldsymbol{L}\vec{n}(\vec{u} + c\vec{n})^T\, ds = \boldsymbol{L}c$$

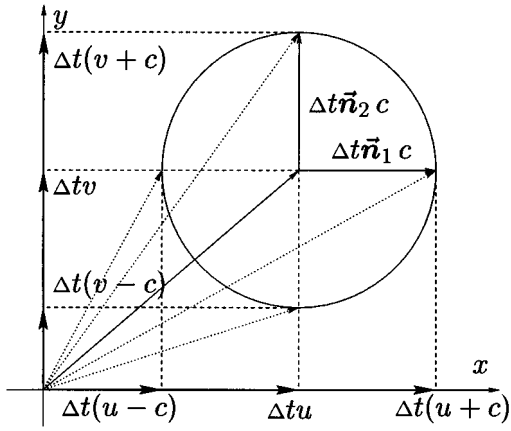

FIG. 2. Actual propagation directions using 1-D operators and four integration points on the Monge cone.

which equals the matrix in (10). This is one advection form of the Euler equations. The presence of the integral reflects that the system is decomposed into infinitely many advection equations. This of course leads to a large amount of computational work in the numerical implementation with little hope of an extension to higher order of accuracy. The integral in (16) over the unit sphere can be approximated by an quadrature rule with given support points $\vec{x}_i$. This directly leads to finitely many propagation directions. In contrast to the splitting approach in (7) and (8), the directions are *not* aligned with the coordinate axes (see Fig. 2). A more general form of the decomposition (16), with finitely many directions, reads

$$(\mathbf{R})_t + \nabla \cdot (\mathbf{R}_2 \vec{\boldsymbol{u}}^T) + \frac{1}{k} \sum_{i=1}^{k} (\mathbf{R}_1 + q\boldsymbol{L}\vec{\boldsymbol{n}}_i)_t + \nabla \cdot ((\mathbf{R}_1 + q\boldsymbol{L}\vec{\boldsymbol{n}}_i)(\vec{\boldsymbol{u}} + \vec{\boldsymbol{n}}c)) = 0. \quad (17)$$

This is a different advection form of the Euler equations.

The consistency relations in [2] become the simple form

$$\mathbf{U} = \mathbf{R}_2 + \frac{1}{k} \sum_{i=1}^{k} \mathbf{R}_1 + q\boldsymbol{L}\vec{\boldsymbol{n}}_i \quad (18)$$

$$0 = \sum_{i=1}^{k} \vec{\boldsymbol{n}}_i \quad (19)$$

$$\frac{k}{q} \boldsymbol{I} = \sum_{i=1}^{k} \vec{\boldsymbol{n}}_i \vec{\boldsymbol{n}}_i^T \qquad \text{or} \qquad \sum_{i=1}^{k} n_{i,j} n_{i,k} = \frac{k}{q} \delta_{j,k}. \quad (20)$$

In two space dimensions, three support points would be enough for the quadrature rule to fulfill the above relations. To retain symmetry between the two coordinate directions, four directions are used. Figure 2 shows the situation with the choice

$$\vec{\boldsymbol{n}}_i \in \left\{ \begin{pmatrix} 1 \\ 0 \end{pmatrix}, \begin{pmatrix} 0 \\ 1 \end{pmatrix}, \begin{pmatrix} -1 \\ 0 \end{pmatrix}, \begin{pmatrix} 0 \\ -1 \end{pmatrix} \right\},$$

where the points are on the Monge cone. With the additional assumption $\|\vec{n}_i\|_2 = 1$, it is clear that $q = N$.

It turns out that it is an advantage to use support points that are outside the Monge cone. The choice

$$\mathbf{n}_i \in \left\{ \begin{pmatrix} 1 \\ 1 \end{pmatrix}, \begin{pmatrix} -1 \\ 1 \end{pmatrix}, \begin{pmatrix} 1 \\ -1 \end{pmatrix}, \begin{pmatrix} -1 \\ -1 \end{pmatrix} \right\} \tag{21}$$

has already been used in ([2]). The piecewise constant function f^c is the superposition of the four waves $\vec{n}_i$. Applying (20) to this decomposition gives $q = 1$, independent of the spatial dimension. It can be shown that this is the only choice of $\vec{n}_i$ that

(a) collapses to the 1-D method for a grid aligned 1-D problem;
(b) has the same time step restriction as the 1-D method, i.e.,

$$\Delta t \leq \frac{\Delta x}{(|u| + c)}.$$

The advection form in (17) allows us to proceed in the same fashion as for the 1-D case in (4). The dependencies are removed by defining the quantities:

$$\begin{aligned} \mathbf{S}_0(\vec{x}, t, 0) &:= \mathbf{R}_2(\mathbf{U}(\vec{x}, t)) \\ \mathbf{S}_i(\vec{x}, t, 0) &:= \frac{1}{k}(\mathbf{R}_1(\mathbf{U}(\vec{x}, t)) + q\boldsymbol{L}(\mathbf{U}(\vec{x}, t))\vec{n}_i), \qquad i = 1, 2, \ldots, k \end{aligned}$$

and the associated velocities

$$\begin{aligned} \vec{a}_0(\vec{x}, t) &:= \vec{u}(\mathbf{U}(\vec{x}, t)) \\ \vec{a}_i(\vec{x}, t) &:= \vec{u}(\mathbf{U}(\vec{x}, t)) + c(\mathbf{U}(\vec{x}, t))\vec{n}_i, \qquad i = 1, 2, \ldots, k. \end{aligned}$$

The corresponding evolution operators are given by

$$\frac{\partial}{\partial \tau}\mathbf{S}_i(\vec{x}, t, \tau) + \nabla \cdot \left(\mathbf{S}_i(\vec{x}, t, \tau)\vec{a}_i^T(\vec{x}, t)\right) = 0, \qquad i = 0, 1, \ldots, k, \tag{22}$$

which reduces the problem to the solution of 20 linear scalar equations. An approximation of the solution at time $t + \Delta t$ is obtained with

$$\mathbf{U}(\vec{x}, t + \Delta t) = \sum_{i=0}^{k} \mathbf{S}_i(\vec{x}, t, \Delta t).$$

Note that even though the basic intention was the derivation of a new multidimensional method, we are now left with a representation of the solution operator for the non-linear Euler equations as a finite sum of linear operators. This representation needs no knowledge of the actual space discretization or of the numerical method used to solve the linear equations. This enables a rigorous error analysis of the splitting error. We will assume in the next section that there is a numerical method that provides the solution of the linear equations to any order necessary for the investigations.

A necessary condition for this decomposition to be stable is the stability of the numerical solution of each linear equation. Assuming that we have a stable method of the linear equation for

$$\max_j \left| \frac{\Delta t a_j^i}{\Delta x_j} \right| < 1$$

if $\vec{a}$ is the advection speed, then the method is stable if the Monge cone lies within the neighboring cells. The scalar method in Section 5 has exactly this property. It turned out that this condition was also sufficient for all the numerical examples we computed.

4. ERROR ANALYSIS

To obtain the error due to the linearization process, we compare the Taylor expansions of the solution in (10) with the sum of solutions in (22) after time Δt. In principle, there is no difference between the expansions in one and two dimensions and therefore we illustrate this process for the equation of mass conservation in the 1-D case only.

For the density after time Δt we get

$$\rho(x, t_0 + \Delta t) = \rho(x, t_0) + \Delta t \rho_t(x, t_0) + \frac{\Delta t^2}{2} \rho_{tt}(x, t_0) + O(\Delta t^3)$$

and with the Euler equations the time derivatives can be replaced by spatial derivatives, i.e.,

$$\begin{aligned} \rho_t &= -(\rho u)_x, \\ \rho_{tt} &= (-m_x)_t = (\rho u^2 + p)_{xx} = \left(\rho \left(u^2 + \frac{c^2}{\gamma} \right) \right)_{xx}. \end{aligned}$$

To advance the solution in terms of the linearized equations we first decompose the density at time t_0 into

$$\rho(x, t_0) = \rho_1(x, t_0) + \rho_2(x, t_0) + \rho_3(x, t_0) \qquad \text{with } \rho_1 = \rho_3 = \frac{1}{2\gamma}\rho \text{ and } \rho_2 = \frac{\gamma - 1}{\gamma}\rho.$$

For each part ρ_i we consider the advection equations

$$(\rho_{1/3})_t + ((u \pm c)\rho_{1/3})_x = 0 \qquad \text{and} \qquad (\rho_2)_t + (u\rho_2)_x = 0,$$

which leads to

$$\begin{aligned} (\rho_{1/3})_t &= ((u \pm c)\rho_{1/3})_x, \\ (\rho_{1/3})_{tt} &= ((u \pm c)((u \pm c)\rho_{1/3})_x)_x, \\ (\rho_2)_t &= -(u\rho_2)_x, \\ (\rho_2)_{tt} &= (u(u\rho_2)_x)_x. \end{aligned}$$

Since $(\rho_1 + \rho_2 + \rho_3)_t = -(u(\rho_1 + \rho_2 + \rho_3))_x = -(u\rho)_x$, the first order part is equal in both cases, which proves consistency. In the second order term we get

$$\rho_{tt} - (\rho_1 + \rho_2 + \rho_3)_{tt} = -\left(\frac{\rho}{2}(\gamma u u_x + c c_x) \right)_x \neq 0 \tag{23}$$

which shows accuracy of first order only.

A closer look at the structure of the coefficients suggests the use of correction terms in the advection equations. The choice of

$$\hat{\rho}_{1/3} = \rho_{1/3} \pm k^{\rho} \qquad \text{with } k^{\rho} = -\frac{\Delta t \rho}{2c}(\gamma u u_x + c c_x)$$

instead of $\rho_{1/3}$ eliminates the error in (23). With

$$\rho(x, t_0 + \Delta t) - (\hat{\rho}_1(x, t_0 + \Delta t) + \rho_2(x, t_0 + \Delta t) + \hat{\rho}_3(x, t_0 + \Delta t)) = O(\Delta t^3),$$

we get a second order approximation in smooth regions of the solution. The same analysis can be done for the other components of the state vector in one dimension and also in the 2-D case. The resulting correction terms are

$$\begin{aligned}
k^{\rho} &= -\frac{\Delta t \rho}{2c}(\gamma u u_x + c c_x), \\
k^{m} &= -\frac{\Delta t}{2}\rho((\gamma - 2) c u_x + u c_x) + u k^{\rho}, \\
k^{E} &= -\frac{\Delta t \rho c}{2\gamma(\gamma - 1)}(u u_x - c c_x) + u k^{m} - \frac{u^2}{2} k^{\rho}
\end{aligned}$$

in the 1-D case and

$$\begin{aligned}
k_1^{\rho} &= -\frac{\Delta t \rho}{2c\gamma}(\gamma(v u_y + u u_x) + c c_x), \\
k_2^{\rho} &= -\frac{\Delta t \rho}{2c\gamma}(\gamma(u v_x + v v_y) + c c_y), \\
k_1^{m} &= -\frac{\Delta t \rho}{2\gamma}(c(\gamma - 1)(v_y + u_x) + v c_y + u c_x - c u_x) + u k_1^{\rho}, \\
k_2^{m} &= \frac{\Delta t \rho}{2\gamma}(c u_y) + u k_2^{\rho}, \\
k_1^{n} &= \frac{\Delta t \rho}{2\gamma}(c v_x) + v k_1^{\rho}, \\
k_2^{n} &= -\frac{\Delta t \rho}{2\gamma}(c(\gamma - 1)(u_x + v_y) + u c_x + v c_y - c v_y) + v k_2^{\rho}, \\
k_1^{E} &= -\frac{\Delta t \rho c}{2\gamma(\gamma - 1)}(u u_x + v u_y - c c_x) + u k_1^{m} + v k_1^{n} - \frac{u^2 + v^2}{2} k_1^{\rho}, \\
k_2^{E} &= -\frac{\Delta t \rho c}{2\gamma(\gamma - 1)}(v v_y + u v_x - c c_y) + u k_2^{m} + v k_2^{n} - \frac{u^2 + v^2}{2} k_2^{\rho}
\end{aligned}$$

in the 2-D case with the special choice (21) for the $\mathbf{n}_i$. In the linearization (22) the matrix $\mathbf{L}$ has to be replaced by $\mathbf{L} + \mathbf{K}$ where $\mathbf{K} = (\mathbf{k}_1, \mathbf{k}_2)$. As mentioned before, the correction terms $\boldsymbol{K}$, depend on the choice of the vectors $\vec{\boldsymbol{n}}_i$ but not on the numerical method used to solve Eqs. (22).

5. NUMERICAL SOLUTION OF THE SCALAR EQUATIONS

The idea of transport applied to a linear scalar conservation law basically governs the behavior of the exact solution. In the constant coefficient case, the equation has the form

$$\omega_t + \vec{\boldsymbol{a}} \cdot \nabla \omega \qquad \text{with } \omega(\vec{\boldsymbol{a}}, 0) = \omega_0(\vec{\boldsymbol{x}}) \tag{24}$$

and the solution is simply the shift with velocity $\vec{\boldsymbol{a}}$, i.e.,

$$\omega(\vec{\boldsymbol{x}}, t) = \omega_0(x - t\vec{\boldsymbol{a}}).$$

In the finite volume context, the quantity

$$\omega_i^n := \frac{1}{|V_i|} \int_{V_i} \omega(\vec{\boldsymbol{x}}, t_n)\, d\vec{\boldsymbol{x}} \tag{25}$$

denotes the averaged value of ω in the control volume V_i. Because of the shift of the solution, the average value ω_i^{n+1} at time $t_n + \Delta t$ is a combination of the values of ω_i^n and all the surrounding neighbors. Figure 3 sketches the behavior if the velocity $\vec{\boldsymbol{a}}$ lies in the upper left quadrant. This behavior is used by other authors to design multidimensional methods. In [1, 6] a representation of this situation by one-dimensional operators is used to extend the idea to the system case.

The situation here is different, since we have already derived a decomposition of the non-linear system into advection equations. All that is left is to design a robust and high order method for a linear scalar equation. Thus, we try to stay as close as possible to the exact solution. For the constant coefficient case (24) we define the contributions to the neighboring cells as

$$F_{i,j} = \int_{V_j} \omega_i(\vec{\boldsymbol{x}} - t\vec{\boldsymbol{a}}, t_n)\, d\vec{\boldsymbol{x}} \qquad \text{with } \omega_i(\vec{\boldsymbol{x}}, t_n) = \begin{cases} \omega(\vec{\boldsymbol{x}}, t_n) & \text{if } \vec{\boldsymbol{x}} \in V_i \\ 0 & \text{else.} \end{cases} \tag{26}$$

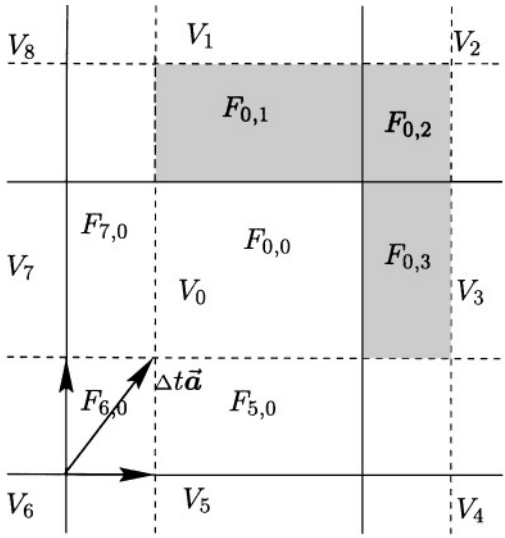

FIG. 3. Propagation of the exact solution in the constant coefficient case.

The value ω_i^{n+1} can be given as

$$\omega_i^{n+1} = \frac{1}{|V_i|} \sum_{j \in \overline{NGB}(i)} F_{j,i} = \omega_i^n - \frac{1}{|V_i|} \sum_{j \in NGB(i)} (F_{i,j} - F_{j,i}), \tag{27}$$

where $\overline{NGB}(i) = \{j \in \mathbb{Z} \mid \bar{V}_i \cap \bar{V}_j \neq \emptyset\}$ and $NGB(i) = \overline{NGB}(i) \backslash \{i\}$ denotes the set of all neighbors of V_i.

The basic problem for all of the finite volume methods in conservation form is that the numerical method defines the cell averages on the new time slice, but it needs a representation of the solution at the old time t_n. To obtain a high order method we first need a high order approximation of the solution $\omega_i(\vec{x}, t_n)$ from the given cell averages ω_i^n and, second, a high order approximation of the integral in (26).

To solve the first problem we use a reasonable reconstruction process $R(\omega^n)(\vec{x}, \vec{x}_i)$ for the function ω from the cell averages ω^n in the neighborhood of $\vec{x}_i$ the center of mass of domain V_i. We define

$$\omega_i(\vec{x}, t) = \begin{cases} R(\omega^n)(\vec{x}, \vec{x}_i) & \text{if } \vec{x} \in V_i \\ 0 & \text{else} \end{cases} \tag{28}$$

or in short form $\omega_i(\vec{x}, t) = R(\omega^n)(\vec{x}, \vec{x}_i)\chi_i(\vec{x})$ with χ_i the characteristic function of volume V_i. From the reconstruction we demand that

$$|\omega_i(\vec{x}, t_n) - \omega(\vec{x}, t_n)| \leq C \Delta x^{p+1} \qquad \text{and} \qquad \int_{V_i} \omega_i(\vec{x}, t)\, d\vec{x} = \omega_i^n$$

if ω_i^n is generated by $\omega(\vec{x}, t_n)$ in (25). The method is of order p if the integration in (26) is of order p, i.e., the error is $C \Delta x^{p+1}$.

Some examples are shown at the end. It is possible to obtain fourth order accuracy for smooth solutions as shown in Fig. 5. Even for discontinuous solutions the fourth order computation shows improvement over first and second order ones.

To solve the resulting linear equations in (22) we need to deal with the variable coefficient case. The equations have the form (11) and the solution can be written in the form (12) with $\vec{z}$ given in (13). If $\vec{a}$ is Lipschitz continuous, the characteristic curves $\vec{z}(\vec{x}_1, t)$ and $\vec{z}(\vec{x}_2, t)$ do not interact for any $\vec{x}_1 \neq \vec{x}_2$ and any $t > 0$. The δ function in (12) models the divergence part of the characteristic curves governed by the ODE:

$$\frac{d}{dt}\omega(\vec{z}(\vec{x}, t), t) = \omega_t(\vec{z}(\vec{x}, t), t) + \vec{a} \cdot \nabla\omega(\vec{z}(\vec{x}, t), t) = -\omega(\vec{z}(\vec{x}, t), t)(\nabla \cdot \vec{a}).$$

Similar to (28) we define a reconstruction $\omega_i^a(\vec{x}, t_n)$ of ω and a polynomial representation $\vec{a}_i(\vec{x})$ of the velocity $\vec{a}$ in each control volume V_i.

Since the equations in (22) result from the linearization of (10) we expect ω and especially $\vec{a}$ not to be smooth. Because of this, we move to a local representation of ω_i and $\vec{a}_i$ possibly discontinuous to neighboring domains. We define as an approximation of the solution $\omega(\vec{x}, t_n + \Delta t)$

$$\omega_i^a(\vec{x}, t, \Delta t) = \int_{\mathbb{R}^N} \omega_i(\vec{y}, t)\delta\left(\vec{x} - \vec{z}_i^a(\vec{y}, \Delta t)\right) d\vec{y},$$

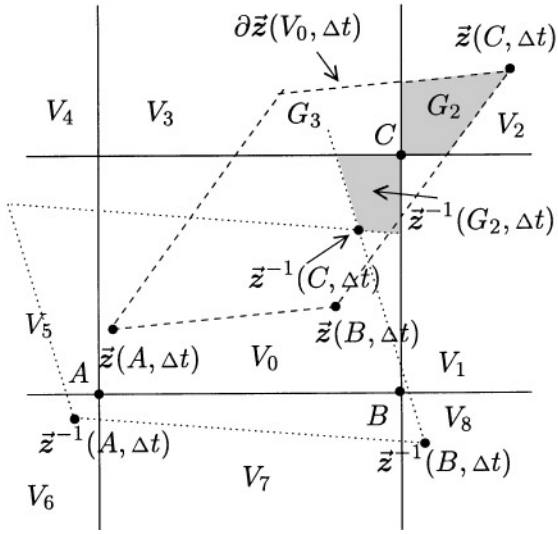

FIG. 4. Relation of forward and backward transformation for domain V_0 and linear varying velocity $\vec{a}$.

where ω_i is defined as in (28) and $\vec{a}_i$ is smoothly extended beyond the domain V_i, so that the solution $\vec{z}_i^a(\vec{y}, \Delta t)$ exists. This models a superposition of adjacent cells.

The computation of the contributions is similar to (26) with

$$F_{i,j} = \int_{V_j} \omega_i^a(\vec{x}, t, \Delta t)\, d\vec{x}. \tag{29}$$

For the update to ω_i^{n+1}, (27) is used.

To achieve second order accuracy, a linear reconstruction for ω and $\vec{a}$ is sufficient. Even though the time integration for $\vec{z}_i^a(\vec{x}, \tau)$ leads to an exponential dependence on τ, the spacial mapping $\vec{x} \to \vec{z}_i^a(\vec{x}, \Delta t)$ for fixed Δt is linear. Thus the boundaries of a rectangular domain V_i remain straight lines (see Fig. 4). Unfortunately, the linear representation of ω_i gets destroyed in the transformation to ω_i^a, which complicates the integration process in (29). For these reasons, it is convenient to use the backward transformation. Formally, the exchange of integration in (29) gives

$$F_{i,j} = \int_{V_i} \int_{V_j} \omega_i(\vec{y}, t)\delta\big(\vec{x} - \vec{z}_i^a(\vec{y}, \Delta t)\big)\, d\vec{y}\, d\vec{x}.$$

The argument of the δ-function is now linear with respect to the inner integration. Quadrature of the δ-function gives a relation between the points $\vec{x}$ and $\vec{y}$ as $\vec{x} = \vec{z}(\vec{y}, \Delta t)$ or $\vec{y} = \vec{z}^{-1}(\vec{x}, \Delta t)$. Under the same assumption on $\vec{a}$ as before, $\vec{y}$ is given by the back transformation of (13) starting from point $\vec{x}$ and can be written as $\vec{y} = \vec{z}(\vec{x}, -\Delta t)$. The contributions then have the form

$$F_{i,j} = \int_{V_i} \omega_i(\vec{z}_i(\vec{x}, -\Delta t), t)\chi_j(\vec{x})\, d\vec{x}.$$

with χ_j the characteristic function of V_j. Figure 4 shows the situation if the velocity $\vec{a}$ is assumed linear in cell i.

The domain G_2 in Fig. 4 is one of the diagonal contributions from V_0 to V_2. The set $\vec{z}(G_2, -\Delta t)$ is the origin of all points that move into G_2 during time Δt. The exponential time dependence needs a second order time integration to keep a second order accuracy in space and time.

Some test calculations for the rotating cone problem using a fourth order method are shown at the end. The fact that the velocity is linear in space is used in this example. A third order reconstruction of ω was sufficient to achieve this result. In general, the implementation is only second order accurate in space and time.

6. NUMERICAL EXAMPLE

The first set of examples illustrates how simple high order accuracy can be obtained for the scalar equations. Figure 5 shows the convergence history for a smooth solution. Initial conditions are in all examples $\omega_0(\vec{x}) = \exp(-|\vec{x} - \vec{b}|^2)$. The triangles and the circles represent the second and fourth order solution of the constant coefficient case with $\vec{a} = (1, 1)^T$. The squares indicate the solution for variable coefficients with $\vec{a}((x_1, x_2)^T) = (-x_2, x_1)^T$. The dashed lines show an exact second and fourth order convergence history.

We use this method to solve the resulting linear equations in (22) for each component. The next example shows the influence of the correction terms. As initial values for this 1-D problem, we use the constant states $\mathbf{U}_L = (3/4, 1, 7/3)^T$ and $\mathbf{U}_R = (1, 1, 3)^T$ from a steady shock for $|x| > 1$. For the values of $|x| < 1$ we pick $\mathbf{U}(x, 0)$ such that $\mathbf{U}(x, 0) \in C^2$, i.e., the initial data are smooth enough. Integration is stopped before the formation of the shock. Table 2 shows the result for the Euler equations. Here, V1 denotes the calculation with correction terms and V2 without them. The estimated error is more than two orders of magnitude smaller for V1 than V2. The L_1 error for V1 shows a nice second order convergence and even the maximum error decays faster than first order. For the steady shock, only one of the characteristic velocities changes sign. Thus only one of the waves has the observed degeneracy of the maximum error. The other waves also have second order convergence in the maximum norm. Without the correction terms, the solution is only of first order in any norm.

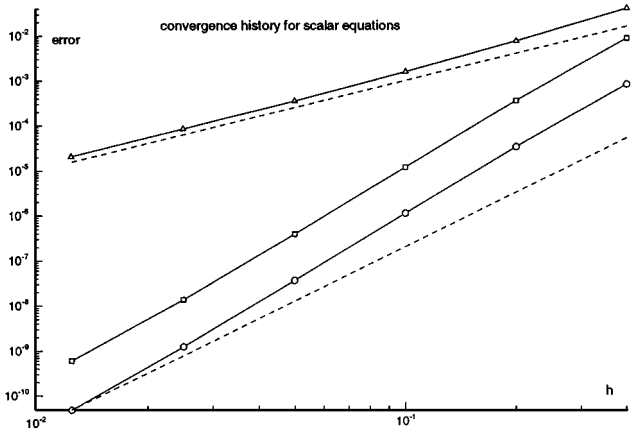

FIG. 5. Convergence history for smooth second and fourth order solutions of a scalar advection equation.

TABLE 1
Convergence History for the Euler Equation with Smooth Data in Two Space Dimensions

Euler equation 2-D				
n	C_0	L_1	Order	
18			C_0	L_1
36	3.8e-2	5.0e-3		
72	2.6e-2	8.3e-4		
144	8.0e-3	1.8e-4	1.704	2.165
288	2.2e-3	2.4e-5	1.879	2.445
576	6.4e-4	6.8e-6	1.768	2.320

The first 2-D example for the Euler equations consists of smooth perturbations in the density, velocity, and pressure. We use $\rho_1 = 1$, $\rho_2 = 1.1$ for the density perturbation, $u_1 = 0$, $u_2 = 0.1$ in the x-velocity, $v_1 = 0$, $v_2 = -0.1$ in the y-velocity, and $p_1 = 1.0$, $p_2 = 0.9$ in the pressure. In the computational domain $[-2, 2]^2$ we used a radial symmetric function to connect the two values. The center of the perturbations is located at $(1/2, 1/2)^T$, $(1/2, -1/2)^T$, $(-1/2, -1/2)^T$, and $(-1/2, 1/2)^T$ for density, x-velocity, y-velocity, and pressure, respectively. Table 1 shows the convergence results. They are similar to the 1-D example.

Next, we come to discontinuous solutions and show the results for the Mach reflection problem in [1]. The physical domain is $[0, 4] \times [0, 1]$ with a spatial discretization $\Delta x = 1/15$ and $\Delta y = 1/20$. The boundary conditions are hypersonic inflow at $x = 0$ and $y = 1$ with the values of ρ, $(u, v)^T$ and p given as $(1, 2.9, 0, 5/7)^T$ and $(5/3, 2.61934, -0.50632, 1.52819)^T$, respectively. At $y = 0$ reflecting boundary conditions are used and at $x = 4$ hypersonic outflow is applied. The upper part of Fig. 6 shows the density contours and the lower part a horizontal cut at $y = 0.525$. The good stability property allows a second order computation of this example without any limiter (see Fig. 6). To obtain a monotone solution nearly any slope limiter will work in this example. Investigations in [3] show that most of the limiters reintroduce a grid dependence on the underlying grid. This is

TABLE 2
Convergence History for the Euler Equations

Euler equation								
	C_0-error		L_1-error		Order			
n	V1	V2	V1	V2	C_0		L_1	
20	5.1e-3	1.1e-2	7.9e-4	1.4e-3	V1	V2	V1	V2
40	2.5e-3	3.8e-3	2.5e-4	5.4e-4	1.041	1.521	1.634	1.354
80	8.4e-4	1.7e-3	5.4e-5	2.6e-4	1.570	1.155	2.228	1.057
160	2.2e-4	9.5e-4	1.0e-5	1.3e-4	1.909	0.845	2.386	0.998
320	6.9e-5	4.9e-4	2.4e-6	6.6e-5	1.700	0.936	2.124	0.977
640	2.2e-5	2.5e-4	5.8e-7	3.3e-5	1.647	0.972	2.026	0.988
1280	7.1e-6	1.3e-4	1.5e-7	1.7e-5	1.622	0.986	1.989	0.992

Note: V1 with and V2 without correction terms.

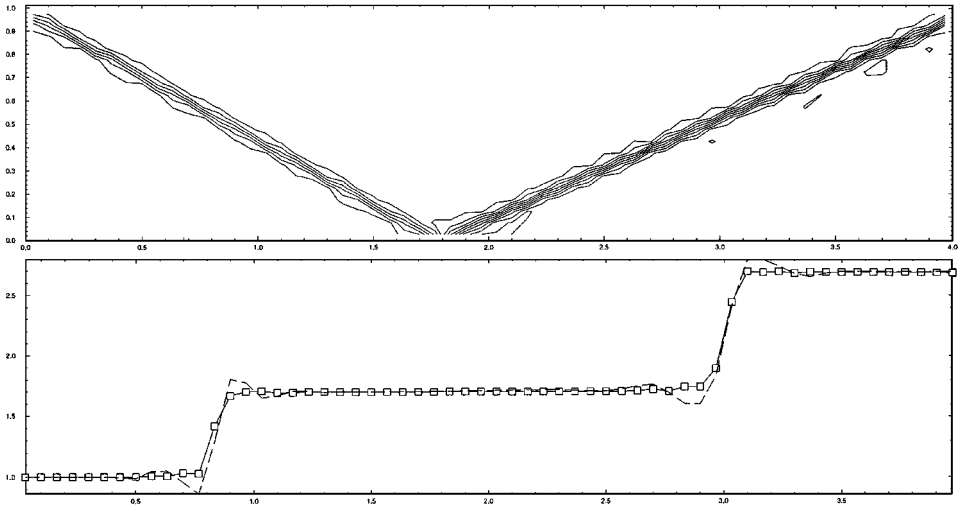

FIG. 6. Density contour lines for the shock reflection problem (upper picture) and density at $y = 0.525$ with and without the limiter (lower picture).

an undesired effect since the method was designed to avoid this effect. Some possible strategies are derived in [3] to solve this problem. Basically two solutions without a limiter are computed: one of first order as a reference and a high order solution. In a next step these solutions, now independent of the grid orientation, are compared to each other, and the "flux," i.e., the contributions, are limited such that newly generated high order extrema do not exceed the first order reference solution. This replaces the direction wise limitation and retains the multidimensional character of the method. The solution is plotted after 300 time steps. The residual is not decreased to machine accuracy due to the limiter function. Without the limiter the solution converges to the steady state with small oscillations close to the shock (dotted line in Fig. 6).

The last problem is the forward facing step problem in [11]. A Mach 3 flow hits a step in the geometry. In the context of the method of transport, the boundary conditions are naturally included for this example. No special treatment of the corner is necessary. The geometry produces a nonphysical peak in entropy close to the corner but this perturbation is local and does not influence the solution downstream as for other methods [5]. The simple shock reflection at the bottom and the almost vertical contour lines of density at the lower left part of the flow indicate no or only a weak entropy layer (see Fig. 7).

7. CONCLUSIONS

The multidimensional linearization of the Euler equations offers a simple way to obtain high order methods that are independent of the space dimensions. The solution of a nonlinear system of equations is reduced to a finite number of linear problems. This provides a better understanding and control of the numerical solution beyond the 1-D Riemann problem. The reduction is independent of the numerical method and the discretization used. The numerical implementation needs to meet the requirement of high accuracy for the scalar case.

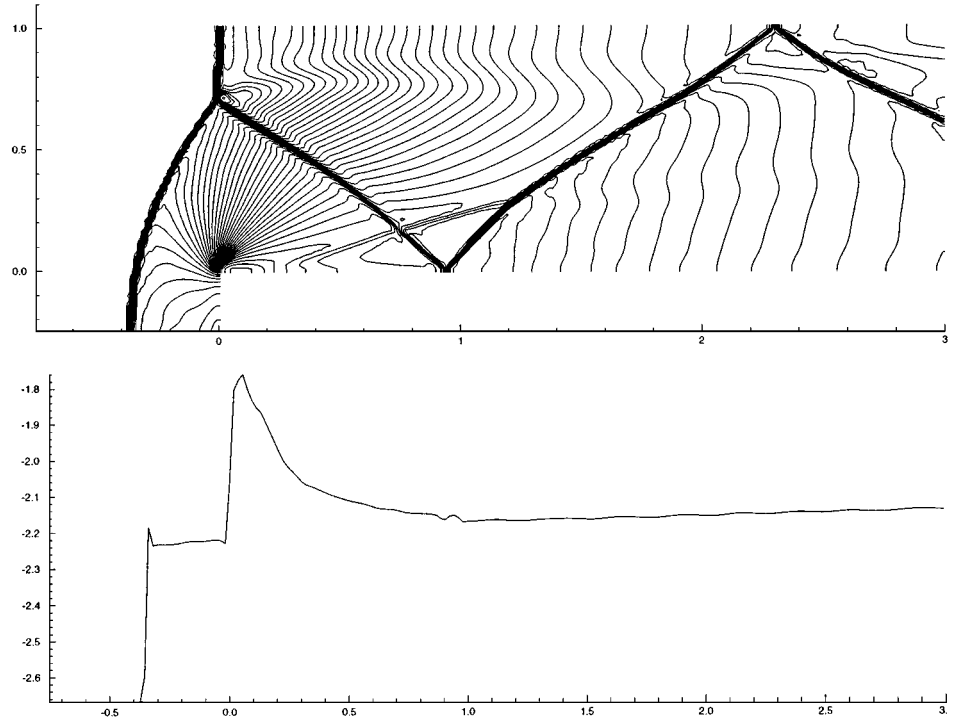

FIG. 7. Solution to forward facing step problem. Density contours (upper picture) and entropy at $y = 0$ (lower picture).

The derivation shows that this linearization can be achieved for any system of conservation laws as long as a decomposition of the state vector and the flux in terms of the MoT is possible. For the shallow water equation there exists such a decomposition as shown in [4] and thus all the results carry over. Application to Navier Stokes [8], plastic-elastic wave propagation, and MHD is in preparation.

REFERENCES

1. P. Collela, Multidimensional upwind methods for hyperbolic conservation laws, *J. Comput. Phys.* **87**, 171 (1990).
2. M. Fey, Multidimensional upwinding. Part I. The method of transport for solving the Euler equations, *J. Comput. Phys.* **143**, 159 (1998).
3. M. Fey, R. Jeltsch, J. Maurer, and A.-T. Morel, *The Method of Transport for Nonlinear Systems of Hyperbolic Conservation Laws in Several Space Dimensions*, Technical Report 97-12, Seminar for Applied Mathematics, ETH Zürich, 1997.
4. M. Fey and A.-T. Morel, *Multidimensional Method of Transport for the Sallow Water Equations*, Technical Report 95-05, Seminar für Angewandte Mathematik, ETH Zürich, 1995.
5. D. Kröner, *Numerical Schemes for Conservation Laws* (Wiley-Teubner, New York, 1997).
6. J. O. Langseth and R. J. LeVeque, Three-dimensional Euler computations using CLAWPACK, in *Conf. on Numer. Meth. for Euler and Navier–Stokes Eq., 1995*, edited by P. Arminjon.
7. R. J. LeVeque, High resolution finite volume methods on arbitrary girds via wave propagation, *J. Comput. Phys.* **78**, 36 (1988).
8. J. Maurer, *The Method of Transport for Mixed Hyperbolic-Parabolic Systems*, Technical Report 97-13, Seminar for Applied Mathematics, ETH Zürich, 1997.

9. J. L. Steger and R. F. Warming, Flux vector splitting of the inviscid gasdynamic equations with application to finite difference methods, *J. Comput. Phys.* **40**, 263 (1981).
10. G. Strang, On the construction and comparison of difference schemes, *J. Numer. Anal.* **5**, 506 (1968).
11. P. Woodward and P. Colella, The numerical simulation of two-dimensional fluid flow with strong shocks, *J. Comput. Phys.* **54**, 115 (1984).
12. H. Yee, *Upwind and Symmetric Shock-Capturing Schemes*, Technical Report TM 89464, NASA, 1987.